Interner Bericht

# DLR-IB-AS-BS-2025-174

# Visualization of flow inside the Fenestron

## Interner Bericht

W. F. J. Olsman[1], J. Lee[2]

Deutsches Zentrum für Luft- und Raumfahrt

[1]Institut für Aerodynamik und Strömungstechnik
Braunschweig
[2]Institut für Robotik und Mechatronik
Oberpfaffenhofen-Weßling

Deutsches Zentrum
DLR für Luft- und Raumfahrt

Deutsches Zentrum
DLR für Luft- und Raumfahrt

# Dokumenteigenschaften

| | |
|---|---|
| Titel | Visualization of flow inside the Fenestron |
| Betreff | - |
| Institut | Institut für Aerodynamik und Strömungstechnik, Abteilung Hubschrauber, Braunschweig |
| Erstellt von | Dr. Ir. W. F. J. Olsman, MSc. J. Lee |
| Beteiligte | - |
| Geprüft von | Dr.-Ing. T. Schwarz |
| Freigabe von | Dr.-Ing. T. Schwarz |
| Zugänglichkeit | ■ Stufe 1: Allgemein zugänglich (in elib ohne Zugangsbeschränkung) |
| | ☐ Stufe 2: DLR intern zugänglich (in elib mit Beschränkung „nur DLR-intern zugänglich“) |
| Datum | 10.11.2025 |
| Version | 1.0 |
| Datei Info | - |

# Visualization of flow inside the Fenestron

**W. F. J. Olsman [1], J. Lee [2]**

[1] Deutsches Zentrum für Luft-und Raumfahrt e.V. (DLR), Institute of Aerodynamics and Flow Technology, Helicopter Department, 38108 Braunschweig, Germany; jurrien.olsman@dlr.de
[2] Deutsches Zentrum für Luft-und Raumfahrt e.V. (DLR), Institute of Robotics and Mechatronics, Perception and Cognition Department, 82234 Weßling, Germany; jongseok.lee@dlr.de

**Abstract**

Flight tests with DLR's EC135-ACT/FHS helicopter were conducted to visualize the flow inside and around the ducted tail rotor (Fenestron) for different combinations of airspeed and side slip. Tufts were fitted on the tail surfaces, inside the diffusor, on the rotor hub and on the stator blades. A second helicopter was flown in close formation with the EC135-ACT/FHS and served as a camera platform to capture the orientation and motion of the tufts. The images were processed with both conventional image processing methods and novel techniques based on deep learning. The results indicate four different flow regimes depending on the combination of airspeed and side slip. An upper/lower asymmetry of the flow inside the duct is observed for positive side slip. Clear reverse flow is only observed inside the duct for low speed and large negative side slip. For other flight conditions the reverse flow is observed indirectly by a flow separation on the inlet lip. The results serve to better understand the complex flow in and around the Fenestron for different flight conditions and can be used for the validation of numerical simulations. Furthermore, the experience gained can be used to apply more complex flow visualization and measurement techniques.

**Keywords:** Helicopter; aerodynamics; ducted tail rotor; Fenestron; flow visualization; tufts

## 1. Introduction

A conventional helicopter needs an anti-torque device to counteract the moment generated by the main rotor. Known solutions for this are, a classical open tail rotor, a NOTAR system or a ducted tail rotor (also known as Fenestron). The application of a Fenestron tail rotor system has the main benefits of a higher efficiency in hover, increased protection against collision with foreign objects and enhanced personnel safety during ground operation, as compared to a conventional open tail rotor. Disadvantages include a reduced dynamic maneuverability, increased weight, complex design and a drag penalty in forward flight. Many of the current Airbus Helicopters light and medium helicopter models are equipped with a Fenestron system. An overview of the development of the EC135 Fenestron can be found in the literature [1,2].

The casing of the Fenestron influences the inflow of the rotor and may be seen as a source of inflow distortion in forward flight. The presence of stator blades inside the duct may cause further distortions due interaction of the rotor with the potential fields around the stator blades or the ingestion of stator blade wakes into the rotor. Distortion or non uniformity of the inflow will cause an increase in noise radiation and a decrease in efficiency. The noise radiation of the Fenestron has been investigated experimentally in the past [3]. This investigation showed that the noise radiation depends on the combination of airspeed and side slip. ONERA and Eurocopter instrumented the Fenestron of a Dauphin

6075 and conducted flight experiments [4]. A technical and financial effort that should not be underestimated. These experiments did not include flow visualization. A wind tunnel experiment investigating the acoustic radiation of a scaled Fenestron model is provided in [5], where a propeller was included in front of the Fenestron to generate vortices that mimic the main rotor wake. Recently Airbus Helicopters build a 1/3 scale model Fenestron to investigate noise mitigation technologies [6]. Although wind tunnel models are very suitable for flow visualization purposes, simultaneous Mach and Reynolds scaling is very difficult to achieve. During steady flight a helicopter is trimmed; the combination of side slip, airspeed and bank angle are all coupled and cannot be varied independently. On the one hand, an isolated Fenestron model in the wind tunnel requires precomputed trim states derived from some aeromechanic simulation of the complete helicopter (or flight test), in order to conduct measurements representative of free flight. On the other hand, a test in the wind tunnel enables the realization of (untrimmed) flight conditions that are impossible to realize in flight. Although one may argue that untrimmed conditions have no practical relevance, they are still scientifically relevant to increase the general understanding of the flow.

The current investigation aims to increase the understanding of the flow in and around the Fenestron for different combinations of airspeed and side slip, by means of flight test. As a first and relatively simple step the flow is investigated by the application of tufts. Tufts are small pieces of wire or rope, taped to a aerodynamic surface [7]. The tufts align themselves with the local flow direction and thereby visualize the local flow direction and topology. Examples of flow visualizations with tufts are available from the literature [8–10].

The results of the current investigation increase the understanding of the flow in and around the Fenestron. They can be used for validation purposes and the gained experience may enable more advanced inflight flow investigation techniques in the future.

## 2. Materials and Methods

This section describes the equipment and methods that were used to obtain the results. First, the helicopter that was used is described, then the materials applied to the helicopter are discussed. Applicable flight limits and considerations are presented at the end of this section.

### *2.1. Helicopters*

The DLR EC135-ACT/FHS helicopter is a highly modified EC135 T2+ helicopter with a unique Fly-by-Light flight control system [11], manufactured by Airbus Helicopters Deutschland, Donauwörth, Germany. The Fenestron is the same as on the series machine, however, the pitch control rod is in a different position and not aligned with the driveshaft, because it is operated by a Fly-by-Light actuator rather than a direct mechanical system. The helicopter is equipped with several modifications, such as a noseboom, which is indispensable for flying with defined side slip. Other useful instrumentation includes several GPS sensors, an inertia platform and the recording of many system parameters such as fuel load, pilot control commands and airspeed.

It was considered to mount two cameras on the end plates of the horizontal stabilizer to capture the motion/direction of the tufts. This would allow a simultaneous view on both sides of the Fenestron and there would be no relative motion between the cameras and the tufts. However, the estimated certification effort was high, the field of view limited and the risk of compromised image quality due to vibrations unknown. Therefore, a different strategy was applied, by deploying a second helicopter as camera platform. For this DLR's Bo105 helicopter was used. This second helicopter was flown in close formation with the EC135 and carried a camera operator that took images of the tail of the EC135. In order

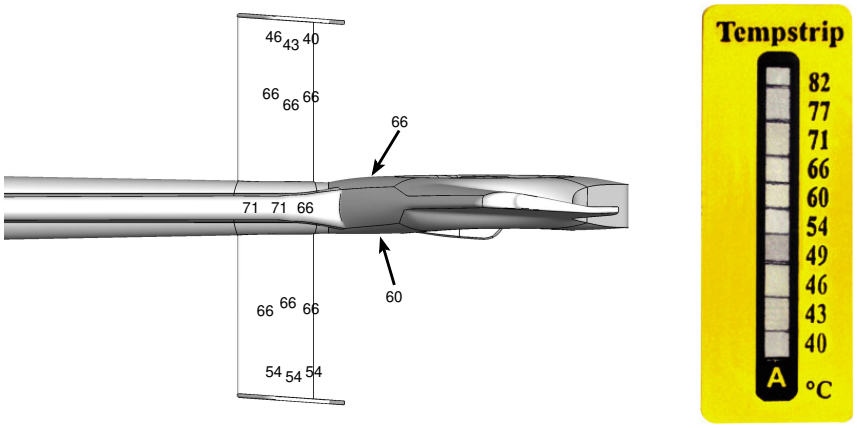


(**a**) (**b**)

**Figure 1.** Maximum temperatures, in °C, at the tail **(a)**. Outside air temperature on ground 10°C. The sketch on the right shows a top view of the tail surface, normal flow direction in forward flight is from left to right. On the right **(b)**, an image of an ATP Messtechnik GmbH RV-101 irreversible temperature sensor is shown.

to allow a sufficient field of view and to the enable a manual tracking of the tail, one side door of the Bo105 was removed. Flight with the Bo105 with a side door removed limits the allowable airspeed to 110 kt. Deploying a second helicopter had the advantage that the Fenestron could be observed from different perspective angles, allowing a view inside the entire duct. Initial tests on the ground, with a 24 Megapixel Nikon D7100 camera with 33–55 mm optic lens, vibration reduction and auto focus, confirmed that at a distance of 50 m, the tufts could be observed with satisfactory resolution. The choice of camera zoom optic was a compromise between accuracy and the ability to manually track the tail inside the camera field of view, while manually compensating for the relative motion between both helicopters during flight. If there is too much zoom one obtains many pixels per tuft, but a slight disturbance will immediately bring the tail outside the field of view of the camera and it will be hard to manually bring it back into the field of view. Time synchronization between the camera and the onboard data acquisition on the EC135 was established by taking photos of the onboard digital clock of the EC135 just prior to take-off. This synchronization is accurate to about 1 s.

### *2.2. Tufts, temperature sensors and markers*

In order to visualize the flow inside and around the duct, tufts were fitted. The tufts were made from black polypropene and were mounted with 3M™ Aluminum Foil Tape 425, which both have a limited temperature resistance. At high temperature the tufts will melt or burn, the aluminum tape will loose adhesive strength. To prevent fire or loss of the tufts, due to hot exhaust gases, RV-101 irreversible temperature sensors from ATP Messtechnik GmbH, were fitted. Figure 1(**b**) shows a temperature sensor, the length of the sensor is about 4 cm and can be pasted to the surface. It is a sensor for discrete temperatures. If the temperature exceeds the given temperature, for about 5 s, the color of the strip at that temperature changes permanently from light gray to black. Initial flight test, with the intended flight conditions (including steady flight with side slip) and with temperature sensors fitted, yielded maximum temperatures at the tail as shown in figure 1(**a**). Knowledge of the maximum temperature at the tail would have also been relevant for possible camera placement, since the considered camera had a maximum operating temperature. The observed left/right asymmetry of the temperature was consistent for all flights and may be related to the rotational direction of the main rotor,

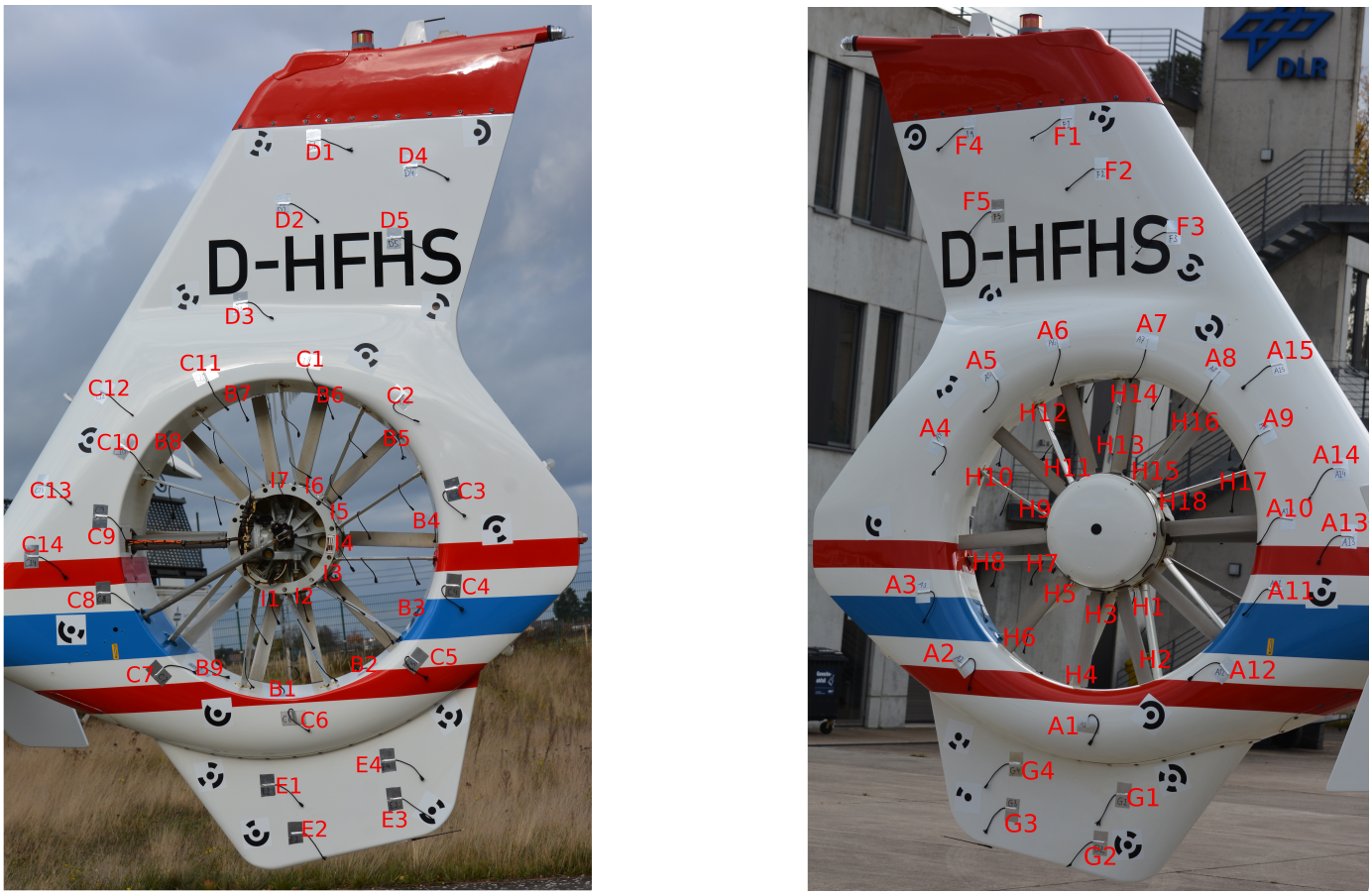


(**a**) (**b**)

**Figure 2.** Tuft locations with their labels, in and around the Fenestron and tail surfaces. On the left side **(a)** and on the right side **(b)**. Also shown are circular encoded markers for automatic image processing.

which causes an left/right asymmetric wake development. In addition to the tufts and temperature sensors, circular encoded markers (see figure 2), printed on certified 3M™ Exterior Aircraft Graphic Film A7322, were applied to enable automatic image processing techniques. An infrared image of the temperature distribution on a part of the tail is provided in figure 5b of [12], but this only applies to forward flight without side slip.

Tufts were placed in and around the Fenestron, as shown in figure 2. The tufts had a thickness of 3 mm. The thickness of the tufts is a compromise between visibility and dynamic response. Thinner, lighter tufts align quicker and better with the flow, but are more difficult to observe. On the left side (figure 2(**a**)) tufts were mounted on the upper fin (area D), the lower fin (area E), around the diffusor outlet on the casing (area C), on the outside of the diffusor (area B) and on the inner hub (area I). On the right side (figure 2(**b**)) tufts were located around the inlet on the casing close to the collector (area A), on the upper fin (area F), the lower fin (area G) and on the stator blades (area H). In total 81 tufts were mounted. In the initial flight test tufts were only placed in areas A, B, C, D, E, F and G. After the initial flight tests additional tufts in the areas H and I were added, as well as the circular encoded markers. Airworthiness of all parts and operations was ensured by certification with the DLR Design Organization and a Permit to Fly.

*2.3. Limits*

Since no specific limits on the side slip were given in the EC135 flight manual, limits were defined in cooperation with the manufacturer Airbus Helicopters Deutschland. This resulted in the allowable quasi-steady side slip as a function of the airspeed, as given by the white area in figure 3. This limit applies to both negative and positive side slip. Positive side slip is defined as the nose of the aircraft pointing to the left with respect to the oncoming flow, as seen by the pilot. In addition to the limit for the side slip as shown in

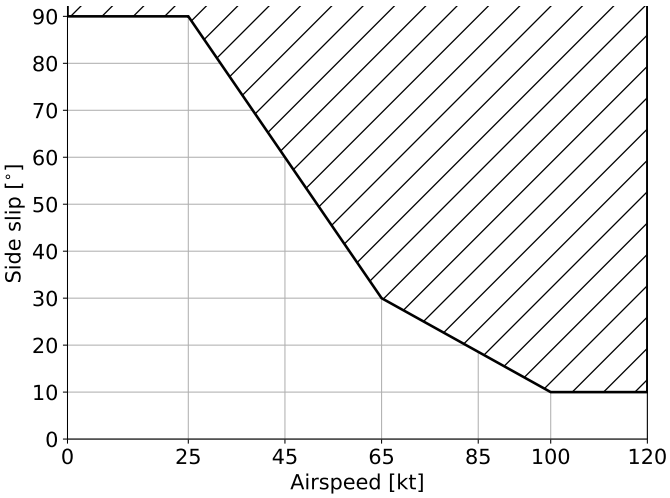


**Figure 3.** Allowable region, in white, for quasi-steady side slip as a function of airspeed.

figure 3, additional limits were defined:

- bank and pitch angles $< 20°$,
- control margin $> 10\%$,
- clear sight of ground,
- 350 m vertical separation from clouds,
- 1500 m horizontal distance from clouds.

Because the Fenestron is located below the main rotor head, there is a significant side slip bank coupling, which at large sideslip angles causes rather large bank angles. Depending on the weight of the helicopter and the current weather conditions it was not possible to reach the side slip limit as defined in figure 3 for all airspeeds, while respecting the required control margin limitation.

Close formation flight with side slip is challenging from a pilot workload point of view and the obvious collision risk. The correct positioning of the follow aircraft with respect to the formation leader is derived by lining up predetermined reference points on the formation leader. However, as side slip is introduced these reference points no longer line up. Furthermore, side slip with the nose of the formation leader pointing towards the follow aircraft gives the optical illusion of being on a collision course.

## 3. Results

It was difficult to assess the quality of the images during flight, therefore camera settings were not always optimal. Also fog/clouds in the background, or the sun appearing from behind a cloud can cause a sudden change in lighting conditions and subsequent over exposure; optimal camera settings are difficult to estimate before flight, while on the ground.

Side slip control is more difficult at low speed due to a decrease in handling and due to the fact that the main rotor downwash affects the noseboom measurement of side slip. For

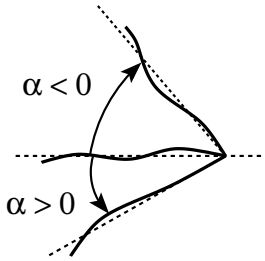


**Figure 4.** Definition of the orientation angle, $\alpha$, of a tuft. Tufts are indicated by the solid black curves and least squares straight line fits are shown by dashed black lines.

typical variations in flight path, pilot controls, airspeed and side slip the reader is referred to the literature [3].

### *3.1. Fully automatic image processing*

Tufts mounted on the vertical fins and inlet (areas A, C, D, E, F and G) can be automatically processed with deep learning methods [13]. An example of the outcome of such a process is given in figure 5. The tufts are recognized by object detection and the objects are automatically labeled A1–A15, F1–F5 and G1–G4. Inside the blue boxes a segmentation is performed that extracts the pixels of the tuft (shown in green). From these pixels the orientation of the tuft can be computed, for instance by a least squares fit of a straight line through the pixels. Other types of curve fitting methods are also possible, which would allow a better captioning of the curved shapes of the tufts, however, a straight line is the simplest. From such a least squares fit an angle with respect to the horizontal can be computed. Since the beginning and end of the tuft is not detected there will be a 180° bias in the angle. This is not an issue as long as the tuft is oriented from right to left in an image of the right side of the Fenestron. A horizontal alignment corresponds to 0°, a tuft points to the upper left corresponds to and angle $< 0°$, and a tuft pointing to the lower left corresponds to and angle $> 0°$. This is illustrated in figure 4 where tufts are shown by solid black curves and least square fit are shown by dashed lines. By computing the orientation of the tufts in several images the motion of individual tufts can be analyzed. The results can be visualized by the mean angle of the tuft and its standard deviation. The mean and standard deviation of the angle of the tuft at location A6 is given in figure 6. For each flight condition (combination of airspeed and side slip) the number of data points for the statistic evaluation varies, because of occlusion or the tuft not being visible in each image that was taken for the specific flight condition. For the data of tuft A6, as given in figure 6, on average about 30 samples are available for the evaluation of statistics. For tuft A6, at a side slip of 0° the mean angle of the tuft decreases with increasing airspeed. This is caused by the fact that the Fenestron thrust decreases with increasing airspeed, such that the tuft is sucked into the duct less for higher airspeed. The standard deviation of the angle of the tuft is low for side slip angles above $-5°$. It can be seen that the tuft is actually pointing upward for side slip angles below $-5°$, which is caused by outflow on the inlet side. It can also be seen that the standard deviation increases with decreasing side slip, indicating increasing unsteadiness. These observations are consistent with the images, such as discussed in the sections below. Similar plots for tufts F1–F5 indicate that the flow on the upper fin is separated for side slip angles below $-25°$. This was identified by a strong increase in the standard deviation of the tufts.

### *3.2. Flow topology*

The tufts inside the duct display a very erratic and unsteady behavior, with overlap, wrapped up shapes and occlusion due to the rotor and stator blades. It would require a

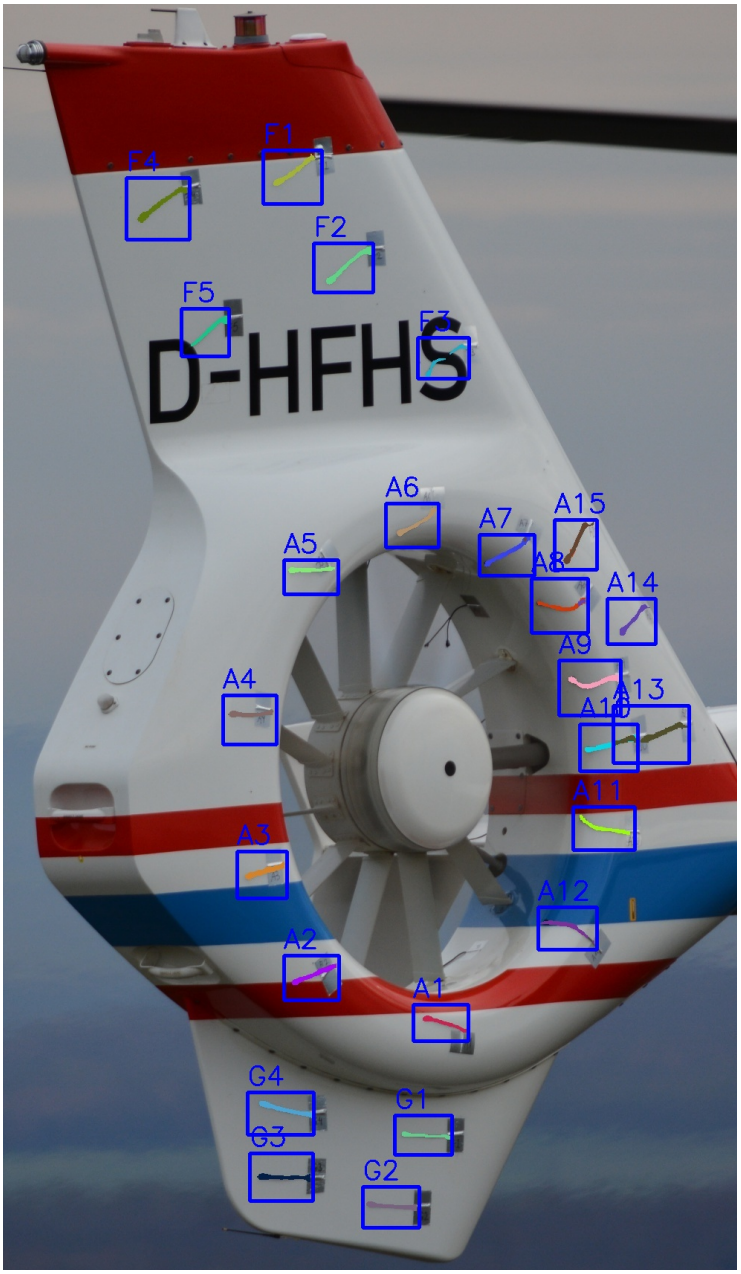


**Figure 5.** Object detection, classification and segmentation of tufts.

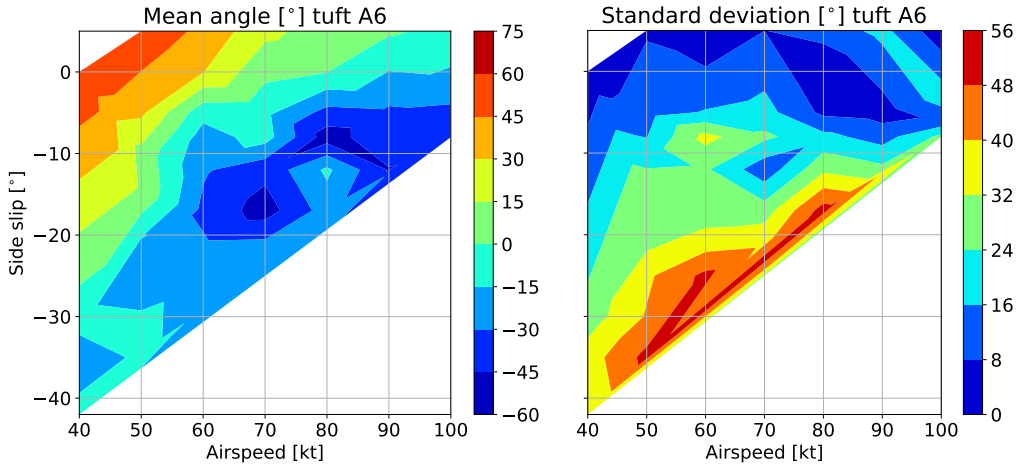


(**a**) (**b**)

**Figure 6.** Mean **(a)** and standard deviation **(b)**, both in degrees, for the angle of tuft A6.

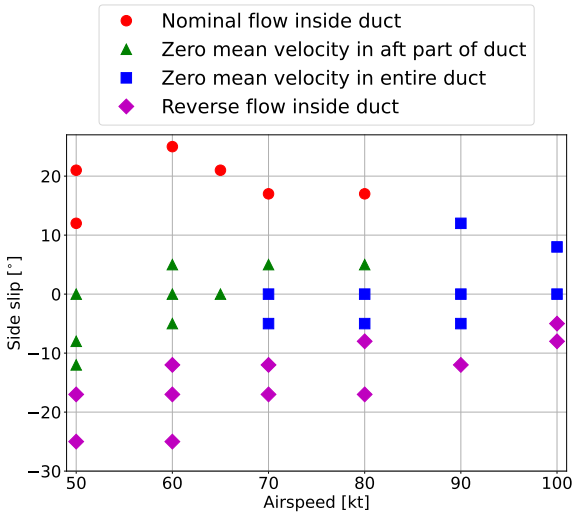


**Figure 7.** Flow topology as a function of airspeed and side slip.

significant labelling and training effort to enable automatic processing of these tufts. The tufts inside the duct were therefore analyzed by conventional image processing techniques. The circular encoded stickers provided enough features to enable a robust affine transformation with 4 degrees of freedom (1 rotation, 2 translations, 1 scaling) of each image to one image from a set of reference images (one for each perspective view). These transformed images provide a stabilized view of the tufts for several images, from which the general motion can be observed. It can be expected that future progress in training strategies for deep learning methods will eventually also enable a fully automatic processing of the tufts inside the duct.

This section describes the main flows in and around the Fenestron duct, depending on the airspeed and side slip. As shown in figure 7, four different regions were identified, the red circles, the blue squares, the green triangles and the purple diamonds. These regions were identified by inspecting a series of images for each flight condition.

3.2.1. Nominal flow inside duct (red circles)

In the region denoted by the red circles the side slip is positive and nominal flow (flow from rotor to stator) through the rotor is expected. Representative images from the series are shown in figure 8, for both the left and right side. For these images the airspeed is

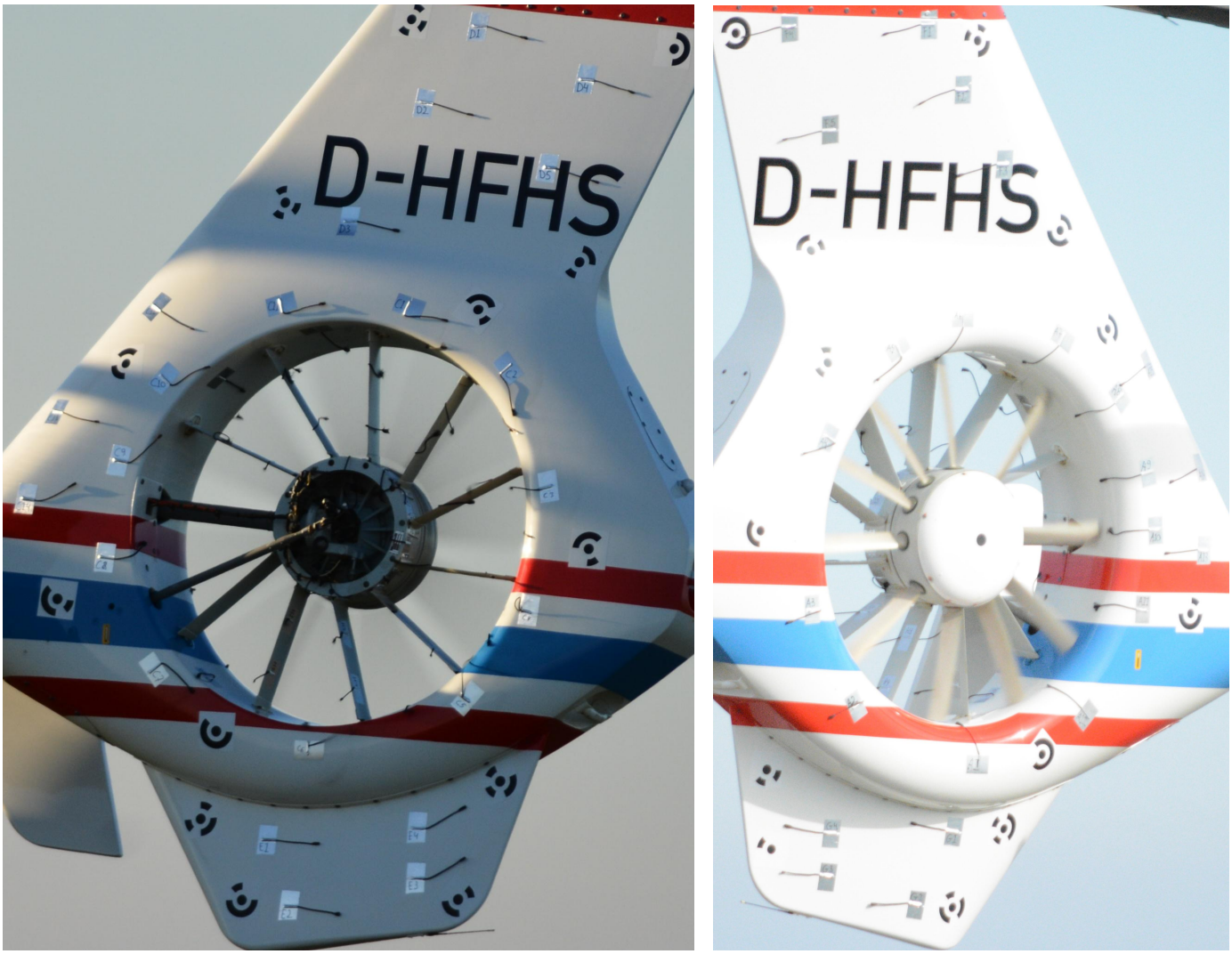


(**a**) (**b**)

**Figure 8.** Flow inside and around Fenestron at airspeed 80 kt and side slip 17°. Seen from the left side **(a)** and from the right side **(b)**. Flow topology marked by red circles in figure 7.

80 kt and the side slip is 17°. The images were not obtained simultaneously. The expected nominal flow is indeed observed in the lower half of the duct, as seen by the alignment of tufts H1–H8, B1, B2 and B9. However, in the upper half of the duct a separated flow is observed between the stator blades, see tufts H9–H18 and B6–B8. All tufts on the hub (area I) display a separated flow. In the forward part of the duct, near the driveshaft there are few tufts, but those that are present (B8 and H17) indicate a separated, low speed flow (dead water area). The upper/lower asymmetry inside the duct may be caused by the

- side slip bank coupling,
- geometry of the casing,
- asymmetric inflow caused by the main rotor wake,
- advancing/retreating blade, the Fenestron blade advancing side is on the bottom and may generate more thrust, compared to the retreating side on the top. Note that the Fenestron rotor has no hinges, such that different blade loading due to advancing/retreating blade sides translates into an induced roll moment.

The leading edge of the upper and lower part of the tail have a sweep angle with respect to the oncoming flow. The sweep angle on the top is different to that on the bottom. A

sweep angle will cause three dimensional streamlines, which can be a source of asymmetric inflow.

Flow visualizations with a smoke generator in a wind tunnel on a small (1:4 scale) isolated Fenestron model also displayed the upper/lower asymmetry. For this wind tunnel model the stator vanes were not present, there was no main rotor, the tip Mach number was a factor 2 lower and the oncoming flow velocity was low to prevent fast diffusion of the smoke. This result indicates that the asymmetry is not caused by the stator blades. This wind tunnel experiment is not further described here.

The tufts in area C display a attached flow on the forward part of the casing, on the aft part C2–C5 an unsteady flow is observed, which indicates that there is nominal outflow in this region.

On the inflow side (right) the flow on the inlet lip is attached for all tufts in area A. Note that tufts A1 and A6 are clearly pointing inside the duct, indicating an inflow. Also on the upper and lower fin (areas D, E, F and G) a steady attached flow is observed.

#### 3.2.2. Zero mean velocity in aft part of duct (green triangles)

The region marked by the green triangles displays a region with small side slip. It is expected that the fin will provide most of the required anti torque and the tail rotor is unloaded. However, since the blades have a high twist and internal recirculating flow can be expected as the inner part of the blades generates nominal flow, whereas the outer part of the blades may generate reverse flow. Images of the flow are shown in figure 9. All tufts in area A are attached and show little movement. Note that both tufts A1 and A6 are not pointing inside the duct as pronounced as was seen in figure 8(**b**). The flow inside the duct appears to be completely separated and no clear flow direction can be observed between the stator blades. The mentioned internal recirculating flow cannot be observed by the tufts. In the lower aft part of the duct the tufts H3–H8 lie still on the surface of the stator blades, which indicates a very low flow velocity (steady attached flow in the direction from hub to casing is unlikely). All other tufts inside the duct display erratic behavior. Tufts on the fins show attached flow. Tufts in area C indicate attached flow, also for C2–C5 a much more stable motion is observed as compared to flight conditions in the region defined by red circles. In figure 9(**a**) it can be seen that tuft C4 is missing. It has been ripped from the aluminum tape. Investigation of the images revealed that the tuft was lost after a flight condition with 90 kt airspeed and a side slip of 12°, see figure 11. Either tuft C4 was subjected to a very high local velocity or the flow was so unsteady that it jerked the tuft through the aluminum tape, the latter appears to be most likely. In subsequent tests tuft C4 was attached with double aluminum tape and was not lost again. At an airspeed of 60 kt and a side slip of 5° the tufts in the lower part of the duct, H1 and H2, are rolled up into spirals, as shown in figure 10. Their shape remains stable for a large series of images, which may indicate the presence of stable vortices. In the upper half of the duct only erratic tuft behavior is observed. This observation again confirms the upper/lower asymmetry of the flow inside the duct, which was also observed for flight conditions in the region marked by the red circles.

#### 3.2.3. Zero mean velocity in entire duct (blue squares)

The state of the tufts for flight conditions in the region given by the blue squares is shown in figure 11. It is expected, at this airspeed, that the vertical fin generates all the anti-torque required for steady flight at 0° side slip. Compared to the region with the green triangles the flow inside the duct is now separated everywhere. No general flow direction can be observed between the stator blades. Tufts in the are A are all attached and display little movement. Tufts A1 and A6 are pointing inward the duct, indicating an inflow into

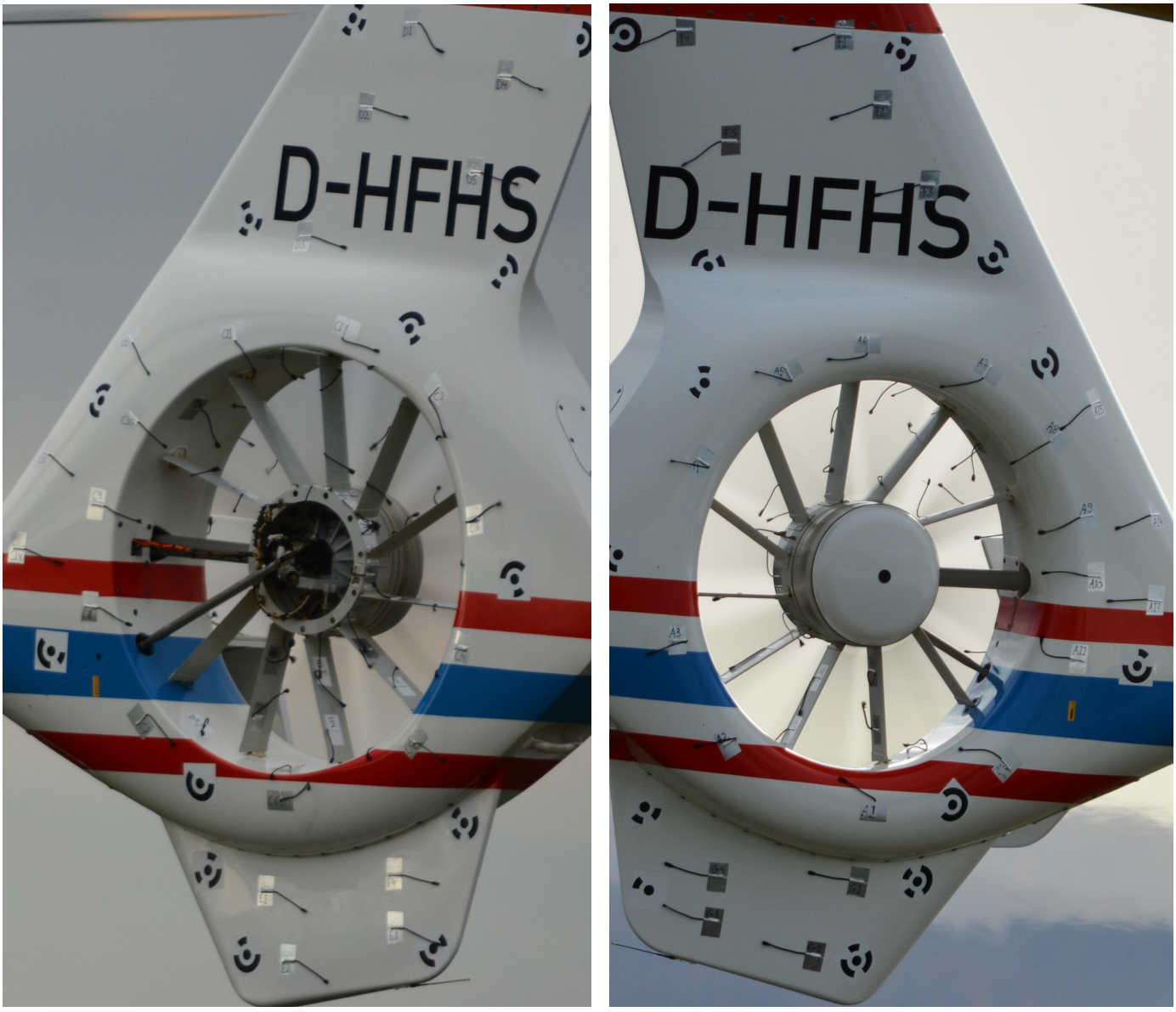


(**a**) (**b**)

**Figure 9.** Flow inside and around Fenestron at airspeed 60 kt and side slip 0°. Seen from the left side **(a)** and from the right side **(b)**. Flow topology marked by green triangles in figure 7.

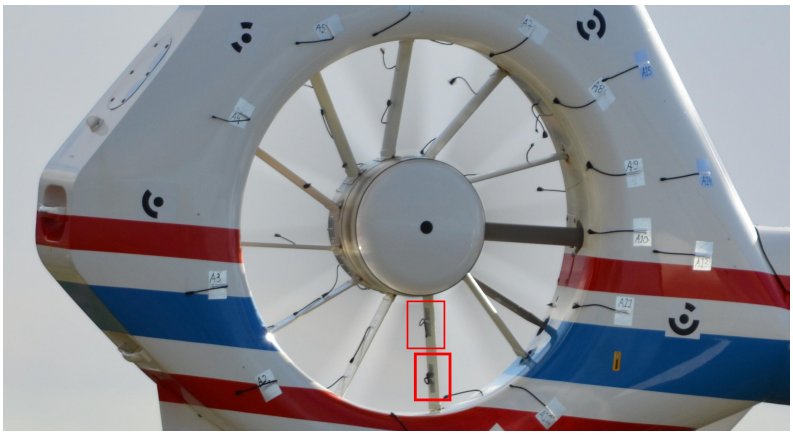

**Figure 10.** Tufts H1 and H2, in the lower half of the duct, rolled up into a stable spiral shape, as annotated by the red boxes. Airspeed 60 kt, side slip 5°.

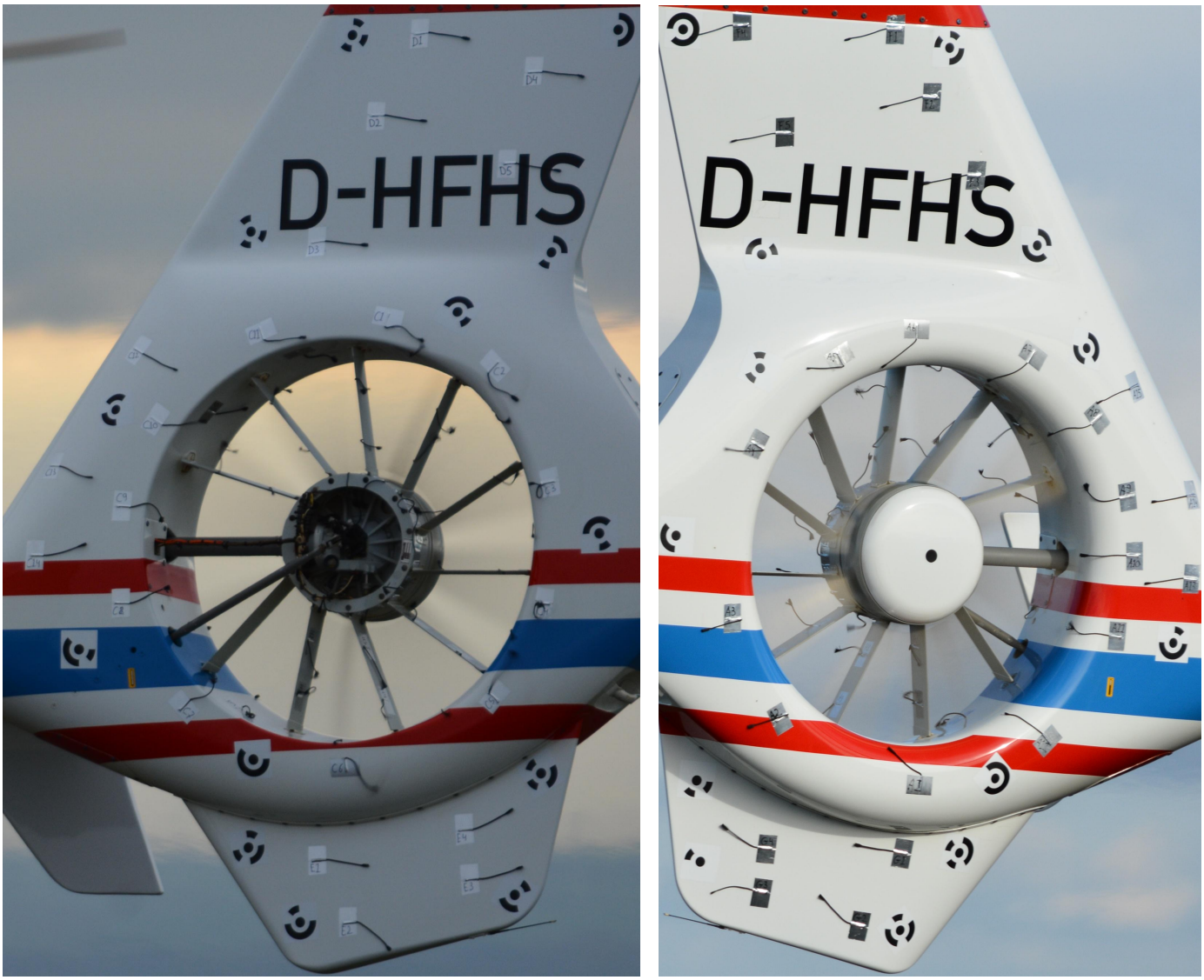


(**a**) (**b**)

**Figure 11.** Flow inside and around Fenestron at airspeed 90 kt and side slip 12°. Seen from the left side **(a)** and from the right side **(b)**. Flow topology marked by blue squares in figure 7.

the rotor. On the left side tufts C2–C5 display a separated unsteady flow. In the image tuft C4 is still attached and displays a rolled up shape.

From figure 15 in [3] it can be seen that for a constant side slip of 5° the Fenestron rotor torque and pedal position are relatively constant with increasing airspeed, for airspeeds above 25 m/s (49 kt). Figure 12 shows the induced velocity $V_i$, the Fenestron power $P_{Fenestron}$, the side force of casing and rotor $T_{Fenestron}$, the side force of the vertical fin $T_{Fin}$ and the pilot pedal command, as a function of the airspeed. These values were obtained from free flight trim at 5° side slip with the flight mechanics code HOST [14]. The computed values are consistent with the experimental results in figure 15 of [3]. At low airspeed the Fenestron rotor must provide all anti-torque. As the airspeed increases the vertical fin produces more and more side force and the side force required by the Fenestron rotor decreases, as does the induced velocity. So with increasing airspeed, the ratio between induced velocity and airspeed decreases. This ratio is important to the flow topology inside the Fenestron duct, which is not unexpected. For a side slip of 5° this ratio is 1 for an airspeed of 45 kt. Below a certain ratio of induced velocity to airspeed the flow topology

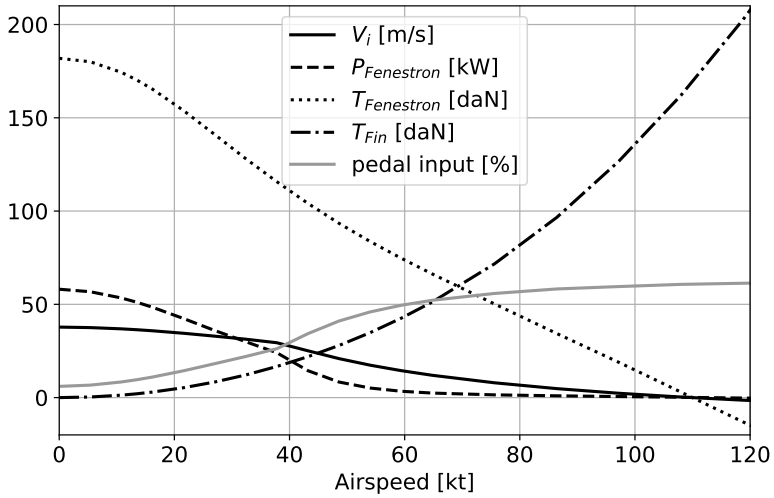


**Figure 12.** Fenestron parameters as function of airspeed for trimmed flight at side slip 5°. Computed with the flight mechanics code HOST [14].

inside the duct changes from zero mean velocity in the aft part of the duct (green triangles) to zero mean velocity in the entire duct (blue squares). The computed values in figure 12, show that at high forward speed at a side slip angle of 5°, the Fenestron rotor can go into windmill brake state. It was not possible to obtain images of the tufts at airspeeds above 110 kt because of a speed limitation of the Bo105 with a side door removed. Obtaining images at high speed was very time consuming (cost intensive) because a lot of flight time was spent catching up with the EC135 and during repositioning.

3.2.4. Reverse flow inside duct (purple diamonds)

For the region indicated by the purple diamonds a reverse flow (from stator to rotor) is expected. Images of the flow are shown in figure 13 for an airspeed of 70 kt and a side slip of $-17°$. This reverse flow is, however, not obvious from the tufts inside the duct. The flow inside the duct appears similar to that of the blue squares region. A very unsteady and unstable flow is observed between the stator blades. Based on the behavior of the tufts inside the duct it is not possible to observe a general flow direction (reverse or nominal). However, tufts in the area A clearly show that the flow there is separated, which indicates that the flow is directed outwards from the inlet lip. Tufts A6 is actually pointing upward and A1 is not sucked into the duct. Tufts A8–A11 also indicate a separated flow and are lifted off the surface. Tufts in the F area indicate some flow separation on the aft part of the upper fin. Tufts in the area G display attached flow. On the left side the tufts in area D and E also display attached steady flow. For a condition with an airspeed of 50 kt and side slip $-25°$, a stable vortex appears in the lower part of the duct, indicated by tuft H2, which is rolled up into a spiral shape. This shape is stable over many images for this flight condition. At an airspeed of 40 kt and a side slip of $-42°$ tufts inside the diffusor are stable and pointing from stator to rotor, which corresponds to reverse flow. However, this conditions was only tested with a reduced number of tufts and was only observed from one side.

## 4. Conclusions

The flow inside the duct of the EC135-ACT/FHS Fenestron was investigated by means of flow visualization with tufts. In total 81 tufts were placed on the upper and lower vertical fin, on the casing, on the inflow and outflow side, inside the diffusor, on the hub and on the stator blades.

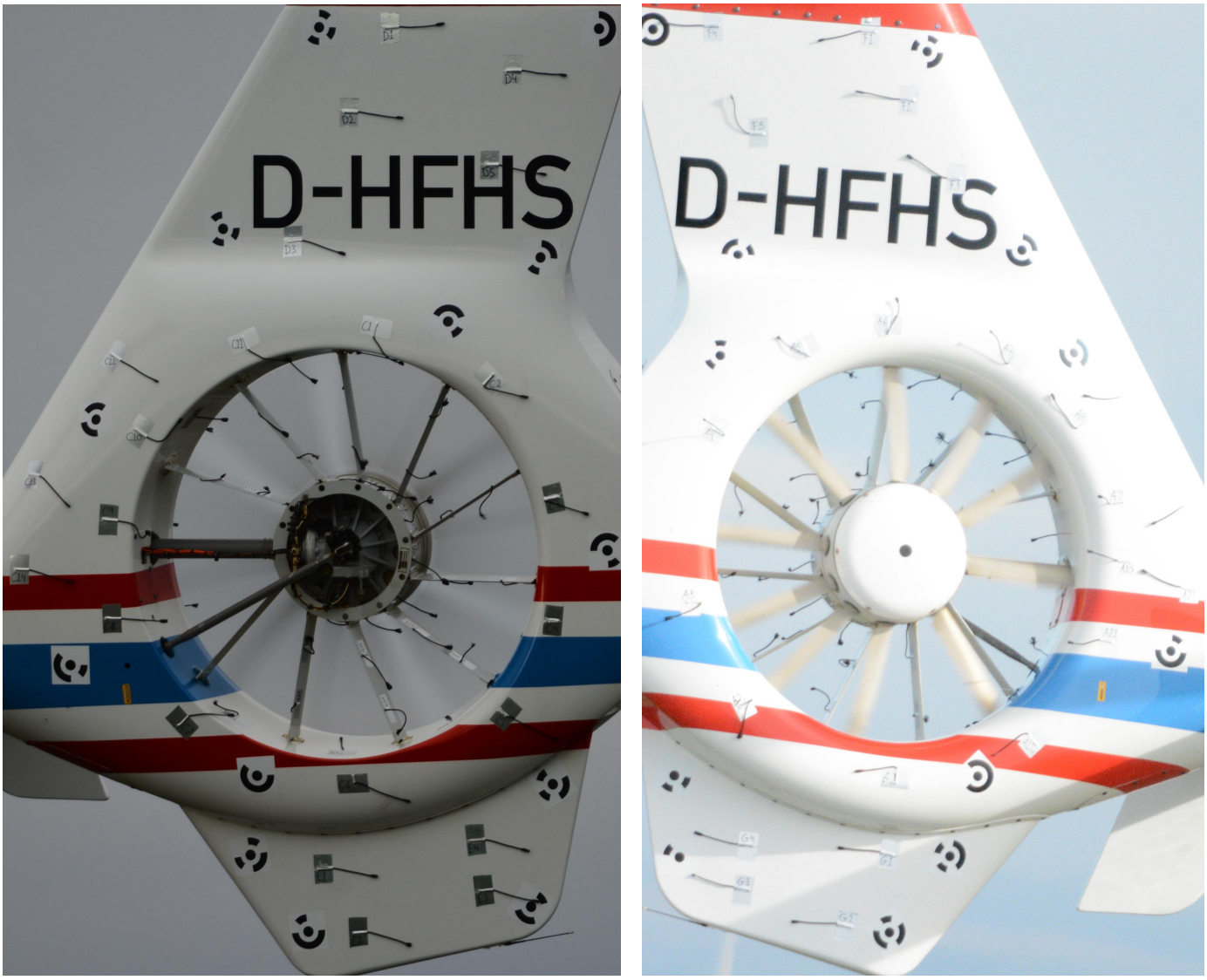


(**a**) (**b**)

**Figure 13.** Flow inside and around Fenestron at airspeed 70 kt and side slip −17°. Seen from the left side **(a)** and from the right side **(b)**. Flow topology marked by purple diamonds in figure 7.

The tufts were observed by a manually operated camera inside a second helicopter flying in close formation with the EC135. Tufts on the vertical fins and on the in and outlet side could be processed automatically with deep learning based methods. This automatic processing enables the quick processing of many images and allows the observation of the behavior of individual tufts over the entire airspeed and side slip range. This comes close to extracting the maximum amount of information possible by the application of tufts. For tufts on the stator blades and in the diffusor fully automatic processing was not successful due to, overlap between the tufts, very erratic shapes and occlusion by stator and rotor blades. The tufts inside the duct were investigated by manually observing a series of (aligned) images for a specific flight condition.

For the tufts inside the duct the flow topology was divided into four regions, depending on airspeed and side slip angle. From the images a clear asymmetry can be observed in the upper and lower part of the duct. Clear nominal flow (flow from rotor to stator) can only be observed in the lower part of the duct and only for large positive side slip angles and airspeeds below 90 kt. Reverse flow can only be observed for very large negative side slip and very low airspeed. For other conditions reverse flow cannot be clearly observed inside the duct, because of the very erratic and unsteady behavior of the tufts. However, on the inlet side of the duct, the effect of reverse flow can be seen as a flow separation on the inlet lip.

Tufts on the inner rotor hub displayed an erratic behavior for most flight conditions and not much information could be retrieved from them. This behavior is caused by the sharp edge at the back of the rotor hub that promotes flow separation. Furthermore, the rotor generates little thrust (low induced velocity) near the rotor hub because of low rotation velocity and the blade shape that transitions from airfoil profile to cylinder. Lastly the flow between the stator blades at the rotor hub is likely three dimensional due to secondary flows in the corners where the stator blades connect to the hub. In addition the visibility of the tufts is complicated by occlusion by stator blades and many features at the back of the rotor hub (stator blade attachments, holes, rivets, etc.).

The results are useful for understanding the flow physics and to potentially further optimize the geometry. The results also provide guidelines for future flight test and help to determine where to place tufts and where to avoid placing them. As general recommendation tufts should be placed at such positions to minimize occlusion, avoid overlap with other tufts and should be observed in clear contrast to the background. It could be considered to utilize a professional stabilized camera system that would capture the tufts with high resolution, this may allow the application of smaller (and therefore more) tufts.

**Funding:** This research was partially funded by the Helmholtz Artificial Intelligence Cooperation Unit (HAICU).

**Acknowledgments:** The authors wish to acknowledge the collegues Miles Barnett, Markus Bernhardt, Elizabeth Buron, Holger Fidelius, Uwe Göhmann, Waldemar Krebs and Sebastian Soffner from the DLR flight experiments department (FX) for their professional support and cooperation during the measurements. Special acknowledgements are expressed to Martin Hepperle and Jörg Meyer for their support in the certification process. Frederic Le Chuiton is acknowledged for helpful discussions and constructive feedback on the first draft of the paper.

## Abbreviations

The following abbreviations are used in this manuscript:

| | |
|---|---|
| ACT | Active Control Technology |
| DLR | Deutsches Zentrum für Luft- und Raumfahrt e.V. |
| FHS | Flying Helicopter Simulator |
| GPS | Global Positioning System |
| HOST | Helicopter Overall Simulation Tool |
| NOTAR | No Tail Rotor |

## References


1. Vialle, M.; Arnaud, G. A new generation of Fenestron Fan-In-Fin tail rotor on EC 135. In Proceedings of the 19th European Rotorcraft Forum. ERF, Cernobbio, Italy, September 1993.
2. Niesl, G.; Arnaud, G. Reduction of the noise signature of the Eurocopter EC 135. In Proceedings of the Flight Vehicle Integration Panel Symposium on "Advances in Rotorcraft Technology". AGARD-CP-592, 7 Rue Ancelle 92200 Neuilly-sur-Seine, France, May 1996.
3. Olsman, W.F.J. Experimental investigation of Fenestron noise. *Journal of the American Helicopter Society* **2022**, *67*, 16–27. https://doi.org/10.4050/JAHS.67.032002.
4. Binet, L.; Cuzieux, F.; Camus, J.C.; Perhuis, L. In-flight and ground instrumentation for Dauphin's Fenestron noise investigation. In Proceedings of the Americal Helicopter Society 66th Annual Forum. AHS international, Fairfax, VA, May 2010.
5. Weisgerber, M.; Neuwerth, G. Influence of a helicopter tail rotor shroud on the interaction noise due to the main rotor vortices. In Proceedings of the 29th European Rotorcraft Forum. ERF, Friedrichshafen, Germany, September 2003.
6. Jauffret, L. Aerodynamic & Acoustic 1/3 rd Scaled Fenestron®. In Proceedings of the American Helicopter Society 81st Annual Forum Proceedings. AHS international, Fairfax, VA, May 2025. https://doi.org/10.4050/F-0081-2025-192.
7. Fisher, D.F.; Meyer Jr, R.R. Flow visualization techniques for flight research. In Proceedings of the AGARD Symposium of the Flight Mechanics Panel on Flight Test Techniques, 1988, number NAS 1.15: 100455.
8. Vey, S.; Lang, H.M.; Nayeri, C.N.; Paschereit, C.O.; Pechlivanoglou, G. Extracting quantitative data from tuft flow visualizations on utility scale wind turbines. *Journal of Physics: Conference Series* **2014**, *524*, 012011. https://doi.org/10.1088/1742-6596/524/1/012011.
9. Wieser, D.; Bonitz, S.; Lofdahl, L.; Broniewicz, A.; Nayeri, C.; Paschereit, C.; Larsson, L. Surface Flow Visualization on a Full-Scale Passenger Car with Quantitative Tuft Image Processing. In Proceedings of the SAE 2016 World Congress and Exhibition. SAE International, April 2016. https://doi.org/10.4271/2016-01-1582.
10. Steinfurth, B.; Cura, C.; Gehring, J.; Weiss, J. Tuft deflection velocimetry: a simple method to extract quantitative flow field information. *Experiments in Fluids* **2020**, *146*. https://doi.org/10.1007/s00348-020-02979-7.
11. Kaletka, J.; Kurscheid, H.; Butter, U. FHS, the New Research Helicopter: Ready for Service. In Proceedings of the 29th European Rotorcraft Forum. ERF, Friedrichshafen, Germany, September 2003.
12. Gardner, A.; Wolf, C.; Heineck, J.; Barnett, M.; Raffel, M. Helicopter rotor boundary layer transition measurement in forward flight using an infrared camera. *Journal of the American Helicopter Society* **2020**, *65*, 2–14. https://doi.org/10.4050/JAHS.65.012002.
13. Lee, J.; Olsman, W.F.J.; Triebel, R. Learning Fluid Flow Visualizations From In-Flight Images With Tufts. *IEEE Robotics and Automation Letters* **2023**, *8*, 3677–3684. https://doi.org/10.1109/LRA.2023.3270746.
14. Benoit, B.; Dequin, A.M.; Kampa, K.; von Grünhagen, W.; Basset, P.M.; Gimonet, B. HOST, a General Helicopter Simulation Tool for Germany and France. In Proceedings of the American Helicopter Society 56th Annual Forum. AHS international, Fairfax, VA, May 2000.